Maniatis, T., Fritsch, E. F., & Sambrook, J. (1982) in *Molecular Cloning: A Laboratory Manual*, Cold Spring Harbor Laboratory, Cold Spring Harbor, NY.
Matthews, B. W., Jansonius, J. N., Colman, P. M., Schoenborn, B. P., & Dupourque, D. (1972a) *Nature (London) 238*, 37–41.
Matthews, B. W., Colman, P. M., Jansonius, J. N., Titani, K., Walsh, K. A., & Neurath, H. (1972b) *Nature (London) 238*, 41–43.
Molineaux, C. J., Lasdun, A., Michaud, C., & Orlowski, M. (1988) *J. Neurochem. 51*, 624–633.
Morales, T. I., & Woessner, J. F., Jr. (1977) *J. Biol. Chem. 252*, 4855–4860.
Oliveira, E. B., Martins, A. R., & Camargo, A. C. M. (1976) *Biochemistry 15*, 1967–1974.
Orlowski, M., Michaud, C., & Chu, T. G. (1983) *Eur. J. Biochem. 135*, 81–88.
Orlowski, M., Michaud, C., & Molineaux, C. J. (1988) *Biochemistry 27*, 597–602.
Orlowski, M., Reznik, S., Ayala, J., & Pierotti, A. R. (1989) *Biochem. J. 261*, 951–958.
Pozsgay, M., Michaud, C., Liebman, M., & Orlowski, M. (1986) *Biochemistry 25*, 1292–1299.
Soubrier, F., Alhenc-Gelas, F., Hubert, C., Allegrini, J., John, M., Tregear, G., & Corvol, P. (1988) *Proc. Natl. Acad. Sci. U.S.A. 85*, 9386–9390.
Stone, K. L., Lopresti, M. B., Crawford, J. M., DeAngelis, R., & Williams, K. R. (1989) *Protein sequence from microquantities of proteins and peptides* (Matsudaira, P., Ed.) Academic Press, New York.
Tisljar, U., & Barrett, A. J. (1989b) *Arch. Biochem. Biophys. 274*, 138–144.
Titani, K., Hermondson, M. A., Ericsson, L. H., Walsh, K. A., & Neurath, H. (1972) *Nature (London) 238*, 35–37.
Towbin, H., Staehelin, T., & Gordon, J. (1979) *Proc. Natl. Acad. Sci. U.S.A. 76*, 4350–4354.
Valee, B. L., & Auld, D. S. (1990) *Proc. Natl. Acad. Sci. U.S.A. 87*, 220–224.

Polarity of Annealing and Structural Analysis of the RNase H Resistant α-5′-d[TACACA]·β-5′-r[AUGUGU] Hybrid Determined by High-Field ^{1}H, ^{13}C, and ^{31}P NMR Analysis†

William H. Gmeiner,‡ K. Ekambareswara Rao,‡ Bernard Rayner,§ Jean-Jacques Vasseur,§ François Morvan,§ Jean-Louis Imbach,§ and J. William Lown*,‡

Department of Chemistry, University of Alberta, Edmonton, Alberta, Canada T6G 2G2, and Laboratoire de Chimie Bio-Organique, UA 488 CNRS, Université des Sciences et Techniques du Languedoc, Place E. Bataillon, 34060 Montpellier, Cedex 1, France

Received April 27, 1990; Revised Manuscript Received July 27, 1990

ABSTRACT: The novel hybrid duplex α-5′-d[TACACA]-3′·β-5′-r[AUGUGU]-3′ was analyzed extensively by 1D and 2D NMR methods. Two forms of the duplex exist in about an 80:20 ratio. Analysis of the exchangeable imino protons of the major component revealed that three AU and one AT base pair are present in addition to two GC base pairs, confirming that the duplex anneals in parallel orientation. The presence of the AT base pair, which can only be accounted for by a parallel duplex, was confirmed by a selective INEPT experiment, which correlated the thymidine imino proton to its C5 carbon. The lesser antiparallel form could be detected by exchangeable and nonexchangeable proton resonances in both strands. An exchange peak was observed in the NOESY spectrum for the thymidine methyl group resonance in both the predominant and lesser conformations, indicating the lifetime of the individual structures was on the millisecond time scale. The nonexchangeable protons of the predominant duplex were assigned by standard methods. The sugar pucker of the ribonucleosides was determined to be of the "S" type by a pseudorotation analysis according to Altona, with the *J*-couplings measured from the multiplet components of the phase-sensitive COSY experiment. The NOE pattern observed for the α-deoxynucleosides also suggested an S-type sugar pucker. The adoption of an S-type sugar pucker for both strands indicates that, in contrast to RNA·DNA duplexes formed exclusively from β-nucleotides, the α-DNA·β-RNA duplex may form a B-type helix. The ^{31}P resonances of the α and β strands have very different chemical shifts in the hybrid duplex and the difference persists above the helix melting temperature, indicating an intrinsic difference in ^{31}P chemical shift for nucleotides differing only in the configuration about the glycosidic bond.

The concept of using antisense oligonucleotides to block gene expression evolved from experiments carried out in the early 1980s. While it was recognized that prokaryotes employ an antisense mechanism to specifically control gene expression, the first demonstration that antisense oligonucleotides could block gene expression selectively in eukaryotic cells was given in studies by Izant and Weintraub (1984). The expression of a thymidine kinase gene injected into mouse fibroblast cells was significantly reduced if a plasmid that directed the production of antisense RNA for the thymidine kinase gene was coinjected.

† This investigation was supported by grants (to J.W.L.) from the Medical Research Council of Canada and the Natural Sciences and Engineering Research Council of Canada and (to J.-L.I.) from CNRS and ARC (France).
* To whom correspondence should be addressed.
‡ University of Alberta.
§ Université des Sciences et Techniques du Languedoc.

0006-2960/90/0429-10329$02.50/0

Interest in the potential applications of the antisense approach to diagnosis and possible therapy of disease states has burgeoned in recent years (Zamecnik & Stephenson, 1978; Zamecnik et al., 1986; Cooney et al., 1988; Miller & Ts'o, 1988; Stein & Cohen, 1988; Strickland et al., 1988; Ts'o et al., 1988; Zon, 1988; Mitchell & Tjian, 1989). Among the problems to be overcome in possible development in this area is that of intracellular degradation of β-oligonucleotide probes by ubiquitous nucleases (Miller et al., 1979; Imbach et al., 1988). We recently reported the synthesis and characterization of a new class of nuclease-resistant oligonucleotide analogues, namely, unnatural α-oligodeoxyribonucleotides, as potential antisense agents (Morvan et al., 1986, 1987a–d; Gautier et al., 1987; Paoletti et al., 1989; Bertrand et al., 1989). These compounds differ structurally from the natural oligomers only by the α-configuration at each anomeric center. Both hyperchromicity and NMR experiments (Gautier et al., 1987; Morvan et al., 1987c,d) confirm that these unnatural oligomers anneal in parallel orientation with complementary β-oligodeoxyribonucleotides as predicted by Sequin from Dreiding models (1973). More recently attention has focused on the annealing of α-oligomer probes with complementary RNA sequences. In experiments with IL6 mRNA sequences it was determined by Northern blot analysis that only parallel-strand (ps) α-oligonucleotides were able to hybridize to the mRNA target (Gagnor et al., 1989). Furthermore only ps α-oligonucleotides were able, in a sequence-specific way, to protect the mRNA target against RNase H mediated hydrolysis or to inactivate the priming capacity of β-oligodeoxynucleotide probes in reverse transcription (Gagnor et al., 1989). Formation of parallel-stranded mRNA·α-oligonucleotide miniduplexes, which prevents hybridization of β-oligonucleotide probes, was considered the most likely mechanism accounting for these results. In view of the significance of α-DNA·β-RNA hybrid formation for the possible application of α-oligonucleotides as gene probes, we considered it essential to obtain structural information on such novel hybrids. Accordingly we report a high-field ^1H and ^{31}P NMR study of the polarity of annealing and structures of the alternative forms of the α-5′-d[TACACA]·β-5′-r[AUGUGU] hybrid.

Materials and Methods

Synthesis. Synthesis of both hexaribonucleotides r(ApUpGpUpGpU) and r(ApUpGpUpGpA) by the phosphotriester method had already been described (Vasseur et al., 1981). After assembling and successive treatments with tetramethylguanidinium 4-nitrobenzaldoximate and aqueous ammonia, the two partially protected hexaribonucleotides, still bearing the acid-labile 2′-methoxytetrahydropyranyl and 2′,3′-methoxymethylene groups, were purified on a DEAE-Sephadex A-25 (Pharmacia) column, lyophilized, and stored at -20 °C as triethylammonium salts.

The hexadeoxyribonucleotide α-d(TpApCpApCpA) was synthesized via a modified phosphotriester method (Morvan et al., 1986, 1987a) whereas α-d(ApCpApCpApT), α-d(TpApCpApCpT), α-d(TpCpApCpApT), and β-d(TpCpApCpApT) were synthesized on solid-phase support by the phosphoramidite method (Morvan et al., 1988). Their homogeneity was ascertained by HPLC analysis using a C-18 reverse-phase column.

Deprotection and Purification of Protected r(AUGUGU). DEAE-Sephadex A-25–120 in chloride form and Dowex-50W 50X8-200 in H^+ form were obtained from Sigma. Triethylamine was from Fisher Scientific Co. and was distilled twice before use. All other reagents used were of analytical grade. Double-distilled water and the apparatus were treated with 1% diethyl pyrocarbonate for 12 h. Then the apparatus was baked at 300 °C for 4 h to destroy RNase. Water was autoclaved (20 min, liquid cycle).

The protected ribonucleotide (25 mg) was dissolved in 0.01 M HCl (16 mL) and the pH was adjusted to 2.0 with 0.1 M HCl. The solution was set aside at room temperature for 6 h and then neutralized with 1.0 M ammonium hydroxide. The sample was loaded on a DEAE-Sephadex (HCO_3^- form) column and eluted with triethylammonium bicarbonate buffer, pH 7.5 (stepwise gradient from 0.001 to 1.0 M). The desired compound came out with 1.0 M buffer. The fractions that have absorbance at 254 nm were collected, combined, and evaporated to dryness under reduced pressure. The residue was dissolved in water (10 mL) and evaporated under reduced pressure to ensure complete removal of triethylamine. The solid was again dissolved in water (5 mL) and passed through a Dowex 50W (Na^+ form) column. The column was eluted with water and the UV 254 absorbing fractions were collected, concentrated, filtered through a 0.45-μm filter, and lyophilized.

Annealing Experiments. Annealing experiments were carried out essentially as described earlier (Paoletti et al., 1989). The buffer used for these experiments was 10 mM cacodylate (pH 7.0) and 1 M NaCl.

NMR Spectroscopy. All NMR experiments were performed on a Bruker cryospectrometer interfaced with an Aspect 3000 computer at 400.13-MHz ^1H frequency at a temperature of 5 °C unless otherwise noted. All experiments performed in H_2O utilized a Redfield 2–1–4 solvent suppressive pulse (Redfield, 1976) with the carrier frequency set 4022 Hz downfield of H_2O and a spectral window of 8333 Hz. The total duration of the 90° pulse was 250 μs. NOE difference experiments consisted of a 1.8-s preirradiation of a single frequency and collection of 8K data points following the 90° pulse. A control spectrum was obtained by irradiation at a frequency near the imino proton frequencies, which contained no resonances. Blocks of 128 scans were collected for both NOE and control spectra and were interleaved until 1024 scans were collected in each experiment. The FID for the NOE spectrum was subtracted from the FID for the control spectrum and the resultant was weighted with 2 Hz of line broadening and Fourier transformed.

Phase-sensitive NOESY experiments (Bodenhausen et al., 1984) with mixing times of 50, 100, and 150 ms were performed in the TPPI mode and consisted of 400 experiments of 48 scans each, a 1.8-s delay between scans in which residual HDO was saturated, and spectral windows in F1 and F2 of 3268 Hz. A phase-sensitive NOESY experiment, with a mixing time of 450 ms consisting of 512 experiments with otherwise identical parameters, was also performed. A 2K × 2K data matrix was obtained by zero-filling in F1 only for a final digital resolution in each dimension of 3.19 Hz/Pt. Data were apodized by sine bells shifted by $\pi/6$ in both dimensions prior to Fourier transformation. Spectra were examined with and without symmetrization about the diagonal but were plotted for publication with symmetrization.

COSY spectra were obtained in both magnitude- (Aue et al., 1976) and phase-sensitive (TPPI) (Marion & Wuthrich, 1983) modes. Broad-band ^{31}P decoupling (Bax & Lerner, 1988) was applied throughout the experiment by using a Bruker B-BM1 broad-band modulator with the decoupling frequency centered at the ^{31}P signal of H_3PO_4 in H_2O and 0.1 W of power. The magnitude spectra were obtained at both 5 and 12 °C and each consisted of 400 experiments of 32 scans. The phase-sensitive COSY experiment was obtained at 12 °C

with otherwise identical parameters. Apodization of the data was by unshifted sine bells in both dimensions while other parameters were as described for the NOESY experiments. Magnitude COSY spectra were also obtained with an additional fixed delay inserted during the evolution time and prior to acquisition of the FID to emphasize long-range couplings (Bax & Freeman, 1981). The fixed delay was set to optimize magnetization due to spins coupled by a 6-Hz coupling constant. These COSY long-range experiments were performed at 5 and 12 °C.

A phase-sensitive ROESY experiment (Kessler et al., 1987) was performed in TPPI mode and consisted of 400 experiments of 48 scans each. Data were zero-filled and apodized as described for the NOESY experiments. A 10% duty cycle was used during the spin-locking time of 200 ms. A 5.2-kHz spin-locking field was used.

One-dimensional ^1H and ^{31}P spectra were obtained at temperatures from 5 to 25 °C in 5-deg increments. Each spectrum consisted of 8K data points over a 3200-Hz spectral window for ^1H and a 1200-Hz spectral window for ^{31}P. ^1H chemical shifts were referenced relative to H_2O at 4.8 ppm and ^{31}P chemical shifts were referenced relative to H_3PO_4 as an external standard at 0 ppm. T1 and T2 relaxation times were measured by the inversion/recovery and by the CPMG methods (Harris, 1983), respectively, and consisted of nine delay times from 8 ms to 2.048 s each. A 10-s delay was inserted prior to each of 32 scans.

A two-dimensional *J*-resolved experiment was performed consisting of 128 experiments of 32 scans each. The F1 dimension was 48 Hz and digital resolution in F1 was 0.37 Hz/Pt. In F2, 8K data points were collected for a digital resolution of 0.25 Hz/Pt.

^1H–^{31}P heteronuclear multiple quantum correlation was obtained with the Bruker spectrometer in inverse mode, using an indirect detection probe. The pulse sequence was that of Bax et al. (1983) and no decoupling was applied during acquisition. The sample was not spinning. A composite 90°–240°–90° was substituted for the refocusing 180° pulse (Shaka et al., 1983). The spectral window in the ^{31}P dimension was 800 Hz and in the ^1H dimension 4000 Hz. A total of 128 experiments of 256 scans were collected for a digital resolution in F1 of 6.25 Hz/point. Digital resolution in F2 was 1.95 Hz/point. Data were apodized by unshifted sine bells in F1 and F2 prior to Fourier transformation. The experiment was optimized for a 10-Hz ^1H–^{31}P coupling.

One-dimensional ^{13}C spectra were obtained by using a 90° pulse and a 1-s relaxation delay. Over a 200 ppm spectral window, 8K data points were collected for digital resolution of 6 Hz/Pt. ^{13}C chemical shifts were referenced to TMS as an external standard at 0 ppm. Selective editing of the ^{13}C spectrum so that only quaternary carbons were detected was accomplished by using the pulse sequence of Bendall and Pegg (1983). Delays were set to optimize suppression of ^{13}C resonances with a 150-Hz C–H coupling. Selective INEPT spectra were obtained by using the pulse sequence of Bax (1984). Only the first 90° pulse was selective with the ^1H channel attenuated to deliver a 30000-μs 90° degree pulse. The evolution delays were set to 25 and 30 ms. The delays were set to optimize polarization transfer without severe losses from T2 effects.

Molecular Modeling. All computations and display of molecular models were done on a Silicon Graphics IRIS 4D-70GT workstation except the program MAKE.DNA, which was run on an Amdahl a5870 computer. Molecular models were displayed by using the program MIDAS from UCSF. Energy minimizations were run by using the CHARMm software package from Polygen. Coordinate files were manipulated by transformation programs written in FORTRAN.

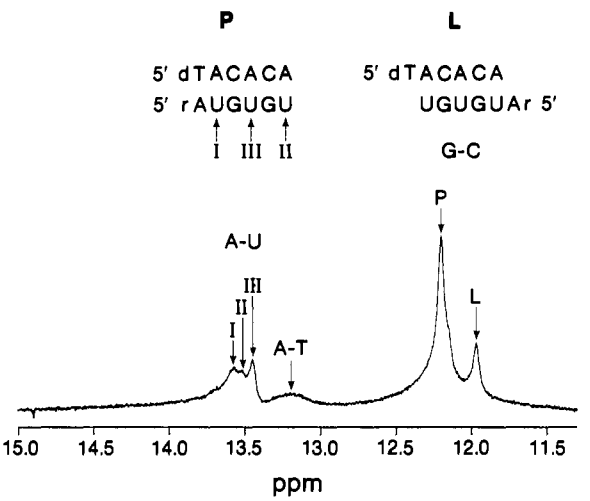

FIGURE 1: ^1H NMR spectrum in 90:10 H_2O/D_2O of the α-DNA·β-RNA hybrid at 5 °C. The spectrum was acquired by using a Redfield 2–1–4 solvent suppressive pulse. The three uridine imino protons from AU base pairs are indicated by Roman numerals. The AT base pair is broadened due to exchange at 5 °C. The two sets of guanosine imino protons are each due to two GC base pairs with the predominant orientation indicated by P and the lesser orientation indicated by L.

Results

NMR Analysis of Exchangeable Protons of α-DNA·β-RNA Hybrid. The proton NMR spectrum at 5 °C (Figure 1) of an equimolar mixture of the two strands in 90% H_2O/10% D_2O clearly indicates four peaks in the region characteristic of uridine or thymidine imino protons based paired with adenosine in Watson–Crick geometry. An analysis of the possible structures for the α-DNA:β-RNA hybrid reveals that if a parallel hybrid duplex is formed four imino resonances from uridine or thymidine are expected while if an antiparallel duplex is formed only three such resonances would occur. If the observed resonances in the imino region of the major component are due to discrete base pairs in the same hybrid structure, the orientation of the hybrid must be parallel, not antiparallel.

The intensity of the resonances of uridine and thymidine imino protons are temperature sensitive. The most upfield resonance is broadened at 5 °C and completely lost to exchange at less than 10 °C. This is consistent with a terminal base pair. The parallel duplex has AT and AU terminal base pairs. The terminal AU base pair is adjacent to a GC base pair and should be thermally more stable than the terminal AT, which is adjacent to an AU base pair. Further support for the assignment of this resonance to the terminal AT base pair is the electron-donating effect of the thymidine methyl group, which shifts the thymidine imino proton upfield of the uridine imino protons. The two most downfield uridine imino protons are next lost to exchange between 10 and 15 °C, while the uridine imino proton, which is the sharpest at 5 °C, is the last to melt. This is consistent with the assignment of the two most downfield resonances to the AU base pairs flanking the GC-AU-GC core of the parallel hybrid duplex while the 13.50 ppm resonance is assigned to the uridine imino proton at the center of this core.

Confirmation of these assignments was obtained by 1D NOE studies of the exchangeable protons in 90% H_2O. Irradiation of the 13.50 ppm uridine imino resonance gave an

NOE to the guanosine imino protons at 12.17 ppm. Further NOEs link the thymidine imino proton at 13.29 ppm to the uridine imino proton at 13.59 ppm at the 5′-end of the parallel hybrid duplex, while the uridine imino proton at 13.66 ppm is assigned to the AU base pair at the 3′-terminus adjacent to the GC base pair at 12.17 ppm.

The region of the exchangeable proton spectrum characteristic of guanosine imino protons base paired to cytidine displays two resonances in about a four to one ratio of intensities (Figure 1). NOE studies indicate that neither of these peaks are from G-U base pairs from a possible β-RNA·β-RNA duplex. The α-DNA sequence displays no self-complementary at all and also contains no guanosine bases, thus the observed resonances must certainly be due to hybrid duplexes. NOE studies confirm that the larger peak at 12.17 ppm is assigned to the GC base pair adjacent to the AU base pair at 13.50 ppm (Figure S1). The relative intensity of the peak allowing for the uneven excitation profile of the Redfield 2–1–4 pulse sequence and intensity variation due to exchange strongly suggests that this resonance is due to two guanosine imino protons degenerate in chemical shift. This resonance is therefore assigned to the two GC base pairs of the parallel duplex.

The absence of NOEs from one GC peak to the other shows that a conformational equilibrium is not in effect but that two distinct species are present in solution. Irradiation of the more upfield guanosine imino resonance results in NOEs to no resonances previously observed although an NOE to 13.47 ppm is observed. This upfield guanosine imino resonance must correspond to the GC base pairs of either an antiparallel hybrid duplex or a second parallel conformation with the uridine imino resonance from the central AU base pair at 13.47 ppm obscured below the 13.50 ppm resonance of the parallel hybrid duplex. Irradiation of the 13.50 ppm uridine imino resonance unavoidably saturates the 13.47 ppm resonance and NOEs are observed to both sets of guanosine imino protons while irradiation of the downfield guanosine imino protons causes an NOE only to 13.50 ppm and irradiation of the upfield guanosine imino protons causes an NOE only to 13.47 ppm.

If the presence of additional peaks in the imino region of the proton NMR spectrum is due to a distinct structure, additional peaks for other resonances of the proton NMR spectrum should also be observed and in the same ratio as is observed for the two sets of guanosine imino protons. This is indeed observed for the well-resolved thymidine methyl group (Figure 2A,B).

The thymidine methyl group is detected in two distinct structures and the minor form has an abnormally upfield chemical shift. Interchange between the two conformations is therefore slow on the NMR time scale, i.e., the interchange rate is slower than the chemical shift difference, which is 240 Hz (0.6 ppm). There is an exchange peak in the NOESY spectrum with a mixing time of 450 ms (Figure 2C) but no exchange peak was observed in the ROESY spectrum with a spin-lock time of 200 ms for the two positions of the thymidine methyl group, indicating that the lifetime of each of the two structures is on the order of hundreds of milliseconds. The upfield shift of the thymidine methyl group (1.0 ppm) in the minor structure indicates some unusual base stacking is present. The presence of a discrete peak for the thymidine methyl group in the minor structure indicates that the latter species is not simply a partially melted form of the predominant structure. A partially melted structure would display broadening of the resonance but not two discrete resonances.

In principle, cross peaks should be observed from each of the species in solution in the 2D experiments but in practice

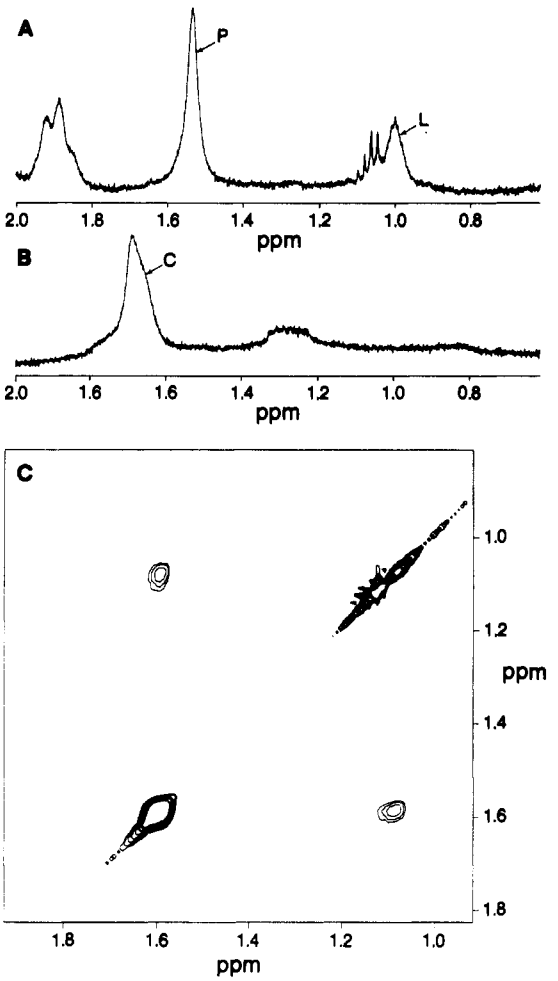

FIGURE 2: Upfield region of the ^1H NMR spectrum of the α-DNA·β-RNA hybrid in D_2O at 5 °C (A) and at 20 °C (B). Two distinct peaks from the predominant (P) and lesser (L) conformations are observed for the thymidine methyl group at 5 °C, while a single broadened peak resulting from coalescence (C) is observed at 20 °C where conformational interchange is rapid. (C) An expansion of the NOESY spectrum at 5 °C with a 450-ms mixing time, showing the exchange peak between the P and L conformations.

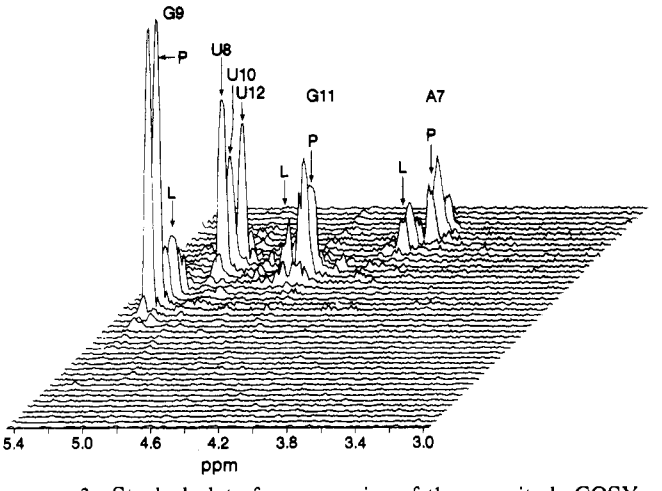

FIGURE 3: Stacked plot of an expansion of the magnitude COSY spectrum about the β-RNA H1′–H2′ region. The nucleotides are denoted by letter and number, while P and L refer to the predominant and lesser orientations of the α-DNA·β-RNA duplex.

the sensitivity of the experiments limits the detection of the lesser component. This is true of most of the 2D experiments run with the exception of the COSY experiment (Figure 3), which displayed strong and weak cross peaks for the predom-

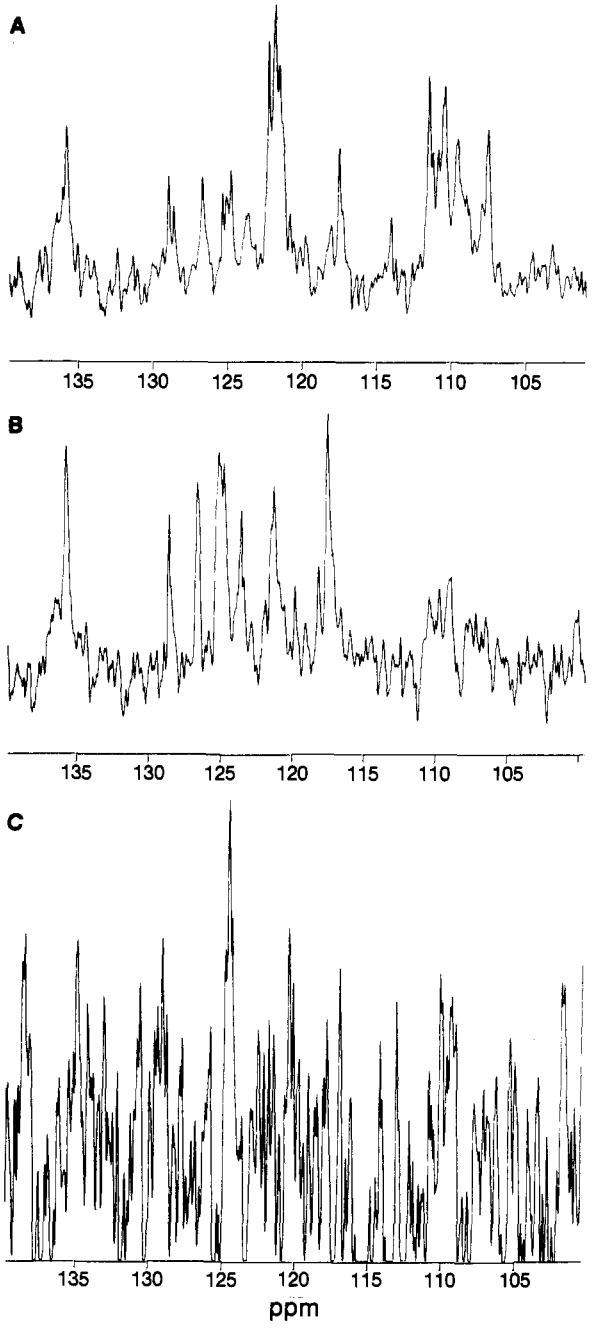

FIGURE 4: ^{13}C observe experiments on the α-DNA·β-RNA duplex. The standard ^{13}C NMR spectrum is shown in (A) while a spectral editing pulse sequence was employed to detect only quaternary carbons in (B). Polarization transfer over three bonds from the thymidine imino proton to the quaternary C5 carbon of thymidine using a selective INEPT sequence is shown in (C).

inant and lesser structures for the H1′–H2′ interactions of the β-ribonucleosides.

In order to verify that the predominant structure has parallel orientation, several ^{13}C observed experiments were run that were designed to determine whether or not the α-thymidine nucleoside was base paired. If it is base paired, the predominant structure must be parallel. The α-thymidine nucleoside is unique in the sequence in being the only pyrimidine with a quaternary C5 carbon. If one of the imino protons could be linked via bond connectivity to the α-thymidine C5 carbon, this would show that the α-thymidine is base paired and that the duplex has the parallel orientation. Three experiments were performed. The first was a one-dimensional ^{13}C observe experiment. The second was a ^{13}C experiment obtained with a pulse sequence tailored such that only quaternary carbons

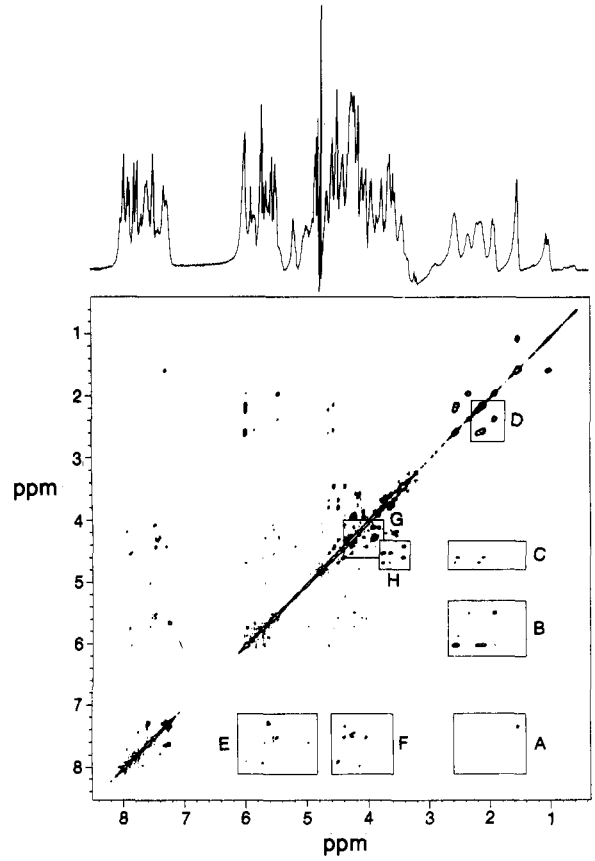

FIGURE 5: NOESY spectrum of the α-DNA·β-RNA duplex at 5 °C with a mixing time of 450 ms. The boxed regions A–H are referred to in the text. Regions A–D, G, and H contain cross peaks only from α-DNA resonances. Regions E and F contain cross peaks from base protons to sugar protons of both the α-DNA and the β-RNA strands.

are observed. The third was a polarization transfer experiment with the most upfield AU (AT) imino proton selectively irradiated and polarization transferred to ^{13}C resonances three bonds away. The results of these experiments are shown in Figure 4. Although the sensitivity of the experiments is not ideal, the spectra do indicate that a single quaternary ^{13}C is the recipient of the polarization transfer from the most upfield AU (AT) imino proton. This imino proton is thus confirmed as the AT imino proton, indicating that the terminal α-thymidine is base paired and that the predominant form of the α-DNA·β-RNA duplex has parallel orientation.

Analysis of the α-DNA Strand of α-DNA·β-RNA Hybrid. The region of the NOESY and COSY spectra that contains cross peaks from the interaction of α-deoxynucleoside sugar and base protons with H2′ and H2″ is devoid of resonances from the RNA strand owing to the absence of H2″ and the relative downfield shift of H2′ in the β-RNA strand. This area is denoted as regions A–D in the full NOESY spectrum shown in Figure 5. Region A contains the base proton to H2′, H2″, and methyl group protons, region B contains the H1′ to H2′ and H2″, region C contains the H3′ to H2′ and H2″, and region D the H2′ to H2″ cross peaks.

The thymidine H6–CH_3 cross peak is identified by its intensity and the upfield chemical shift of the single methyl group in the spectrum. The neighboring adenosine, A2, also displays an NOE from its base proton, H8, to the thymidine methyl group, establishing the connectivity between these two nucleosides (Figure 6). Both T1 and A2 display NOEs from their respective base protons to their own H2′ and they are unique among the α-nucleosides in this respect, although at slightly elevated temperatures (10–15 °C) A_4, C_3, and C_5 also

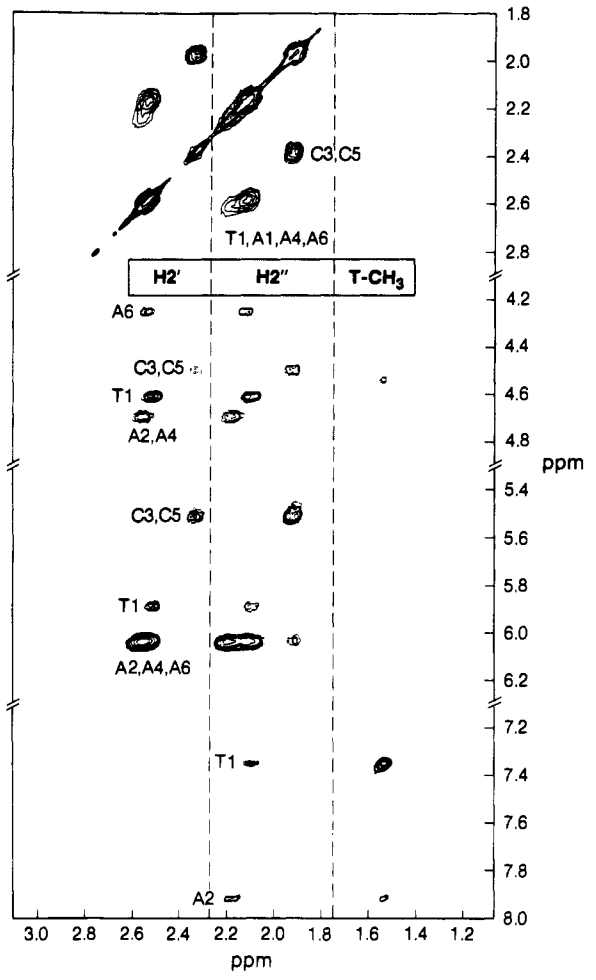

FIGURE 6: Expansion of the NOESY spectrum about the upfield region showing the NOE cross peaks from base protons, H1′, and H3′ to both H2′ and H2″ and to the thymidine methyl group.

show base proton to H2′ NOEs. No NOEs from base protons to the H2′ of neighboring nucleosides were observed for any of the α-nucleosides.

Region B contains the cross peaks due to NOEs between H1′ and both H2′ and H2″. Sets of peaks are observed at three distinct frequencies of the H1′ position, indicating there is some degeneracy in the values of the H1′ chemical shift for the six α-nucleosides. The most downfield H1′ chemical shift at 6.01 pm is shared by A2, A4, and A6. That there are indeed cross peaks from three nucleosides is shown by analyzing the row of the 2D NOESY spectrum that contains the cross peaks. The H1′ to H2′ and H2″ interactions from the two cytidines, C3 and C5, are also overlapped, while the interactions from T1 are well resolved.

The α-deoxynucleosides display strong interactions from both H1′ and H3′ (regions B and C) to H2′ and H2″. The assignments agree with those made for H1′ in region B except that A6, which has the most downfield H1′ chemical shift, has the most upfield H3′ chemical shift. This is consistent with its being the 3′-terminal nucleoside.

The H2′ to H2″ interactions are grouped into two cross peaks. The more upfield cross peak is due to the two α-cytidine H2′–H2″ interactions, while the more downfield peak is due to H2′–H2″ interactions from T1, A2, A4, and A6. In Figure 6 regions A–D of the NOESY spectrum are shown and the chemical shift assignments are presented.

An analysis of just the most upfield region of the NOESY spectrum establishes the H1′, H2′, H2″, and H3′ connectivity for all six α-nucleosides and the base proton connectivity as well for the two α-nucleosides at the 5′-terminus. The remaining base to sugar connectivity assignments are made from an analysis of the base proton to H1′ region of the NOESY spectrum (region E). The two cytidine H6 to H1′ cross peaks fall just downfield of their corresponding H6 to H5 cross peaks. Unfortunately, the β-uridine H6–H5 and H5–H1′ fall very near the corresponding peaks from the α-cytidine nucleosides, making this region of the spectrum very crowded (Figure S2). The α-cytidine resonances are distinguishable on the basis of NOESY cross peaks from H1′ to H2′ and H2″ (vide supra). The remaining base protons are assigned on the basis of the known H1′ chemical shifts of the α-nucleosides and, in the case of T1 and A2, and of C_3, A_4, and C_5 at higher temperature NOEs from the base proton to H2′. Only two interresidue base protons to H1′ NOEs are observed, from the adenosines followed by cytidines.

The H4′ resonances were assigned for each α-deoxynucleoside on the basis of strong intranucleotide NOEs from the base proton to H4′ in region F. The NOE from the base proton to H4′ has been observed previously in duplexes containing α-deoxynucleoside (Morvan, 1987). The conformation about the glycosidic bond must be at least weakly anti for such an NOE to be observed even in NOESY spectra with short mixing times. NOEs from the base proton to H2′ are apparent only for the two nucleotides at the 5′-terminus, and even for these nucleotides the NOE from the base proton to H4′ is the strongest base proton to sugar proton NOE. This indicates that the sugar conformation must be close to a C2′-endo conformation. The pattern of NOEs expected in a C2′-endo conformation for a strand of α-DNA is entirely different than that of the corresponding β-DNA. β-Deoxynucleosides adopting a C2′-endo sugar pucker display strong intranucleotide NOEs from their base protons to H2′ (Hare et al., 1983) because the C2′-endo sugar pucker brings the H2′ proton up toward the base. This same sugar pucker for an α-nucleoside causes the H2′ proton to move away from the base proton to a distance where an NOE may not be observed. The H4′ proton moves closer to the base proton to an NOE observable distance. The assignment of H4′ on the basis of NOEs from the base proton may be verified by NOEs from H4′ to H3′ in region G of the NOESY spectrum. This also provides a check on the H1′ and H3′ resonances previously assigned on the basis of NOEs to H2′ and H2″.

The α-DNA strand displays unusually strong H3′–H5′ NOEs, which make the assignment of the H5′ resonances straightforward. These interactions are found in region H of the NOESY spectrum, which is shown expanded in Figure S3. The H5′ resonances are well resolved even in cases where the H3′ resonances overlap and clearly indicate the number of interactions represented by the H3′–H2′ and H3′–H2″ cross peaks. A strong NOE is also observed between H5′ and H4′ and cross peaks due to these interactions also are shown in Figure S3. The H4′ chemical shift values determined in this way agreed in every case with those obtained from the aromatic proton to H4′ NOE. This indicates that all the NOEs observed are due to intraresidue interactions and ensures that assignments made on the basis of different interactions are self-consistent. The chemical shift values for the α-DNA strand are summarized in Table I.

Assignment of the β-RNA Strand of the Hybrid. The observation of NOEs from H3′ and from H1′ to both H2′ and H2″, which made assignment of the α-DNA sugar resonances straightforward, is not possible in the β-RNA strand. Two factors in addition make the assignment of the β-RNA strand more difficult. One difficulty is that the resonances of the

Table I: Summary of Chemical Shift Assignments in the α-DNA·β-RNA Hybrid

	H8/H6	H5	H1′	H2′	H2″	H3′	H4′	H5′	CH3
T1	7.39		5.95	2.48	2.05	4.60	4.41	3.41	1.58
A2	7.93		6.02	2.59	2.18	4.71	4.57	3.61	
C3	7.53	5.58	5.50	2.18	1.92	4.45	4.36	3.48	
A4	7.98		6.02	2.60	2.20	4.71	4.57	3.79	
C5	7.53	5.58	5.50	2.18	1.92	4.45	4.36	3.48	
A6	8.01		6.02	2.58	2.15	4.22	4.19	3.56	
A7	7.61		5.82	4.60		4.97	4.38		
U8	7.58	5.68	5.81	5.12		4.99	4.39	3.92	
G9	8.11		6.00	5.33		5.16	4.41		
U10	7.59	5.68	5.81	5.12		4.99	4.39	3.92	
G11	8.05		5.85	5.18		4.54	4.31		
U12	7.56	5.70	5.81	5.12		4.99	4.39	3.92	

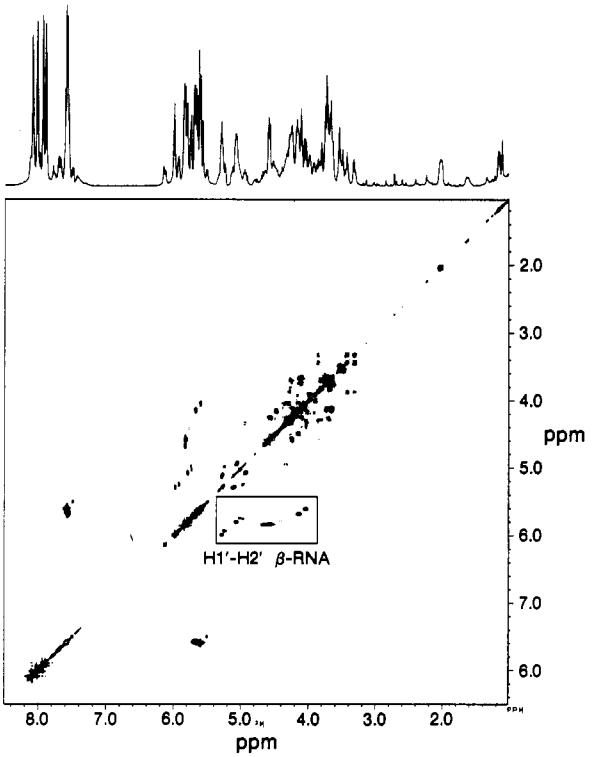

FIGURE 7: Magnitude COSY spectrum of the α-DNA·β-RNA duplex at 5 °C in D_2O. The boxed region denotes the H1′–H2′ cross peaks from the β-RNA strand.

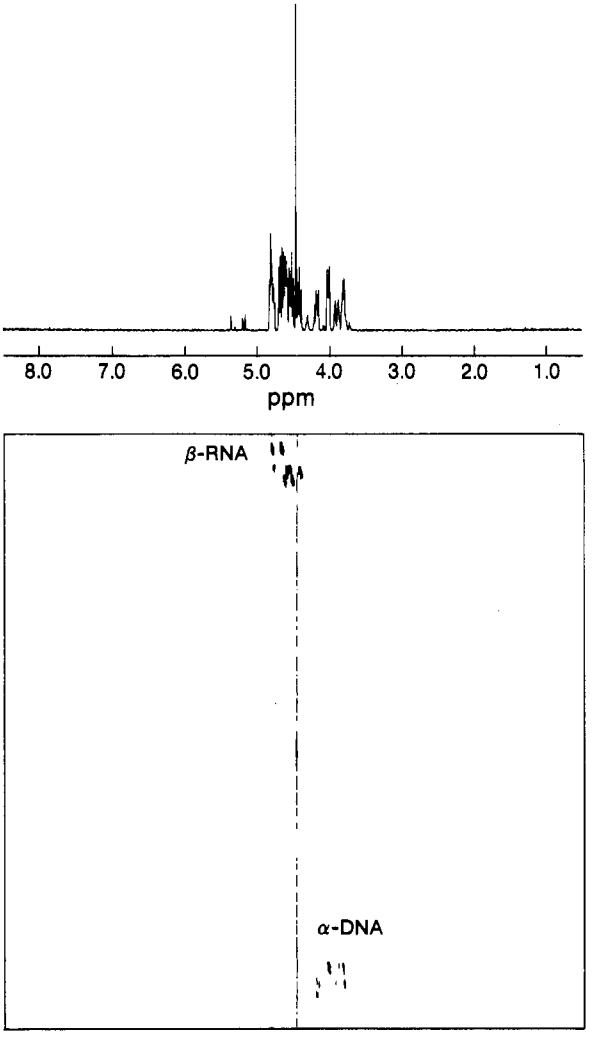

FIGURE 8: ^1H detected ^1H–^{31}P chemical shift correlation spectrum of the α-DNA·β-RNA duplex with use of the HMQC pulse sequence. Only interactions from H3′–^{31}P are observed for both the α-DNA and the β-RNA strands. The cross peaks for the individual strands are well resolved according to both ^1H and ^{31}P chemical shifts. Five major interactions for the predominant species are observed for each strand as well as several cross peaks due to the lesser species.

sugar protons are not as well separated according to proton type, while the second is that the intensity of the cross peaks in the NOESY spectrum for the β-RNA strand is reduced relative to the intensity for the same interactions in the α-DNA strand. An exception to this observation is that relatively strong NOEs are observed from the aromatic protons of all β-RNA nucleotides to H1′ and in some cases to H2′ and H3′ of the corresponding sugar. Observance of base proton to H2′ and H3′ NOEs in the β-RNA strand indicates that the constituent nucleotides do not adopt a strongly syn configuration about the glycosidic bond.

The assignment of the ^1H resonances of the β-RNA strand begins with an analysis of the aromatic proton to H1′ region of the NOESY spectrum. There is no distinction on the basis of chemical shift for either the base protons or the H1′ resonances of the α-DNA and β-RNA nucleotides. The β-RNA resonances in this region are identified through observation of NOEs from the same base proton to H2′ and also a scalar correlation from the COSY spectrum (Figure 7) from H1′ to H2′. There are no NOEs observed between base protons and sugar protons of neighboring nucleosides, indicating either distortion from conventional helix geometry or unusual relaxation properties in certain regions of the structure.

The H3′ resonances of the β-RNA strand fall within 0.5 ppm downfield of water as indicated by the ^1H–^{31}P shift correlation experiment (Figure 8). Correlation of the H2′ and H3′ resonances of the β-RNA strand was accomplished by observation of the corresponding cross peaks in the COSY spectrum shown in Figure 7.

The assignment of the proton resonances of the α-DNA strand was accomplished through interpretation of the NOESY spectra because the α-DNA strand has many strong interactions that fall into regions of the spectra free from res-

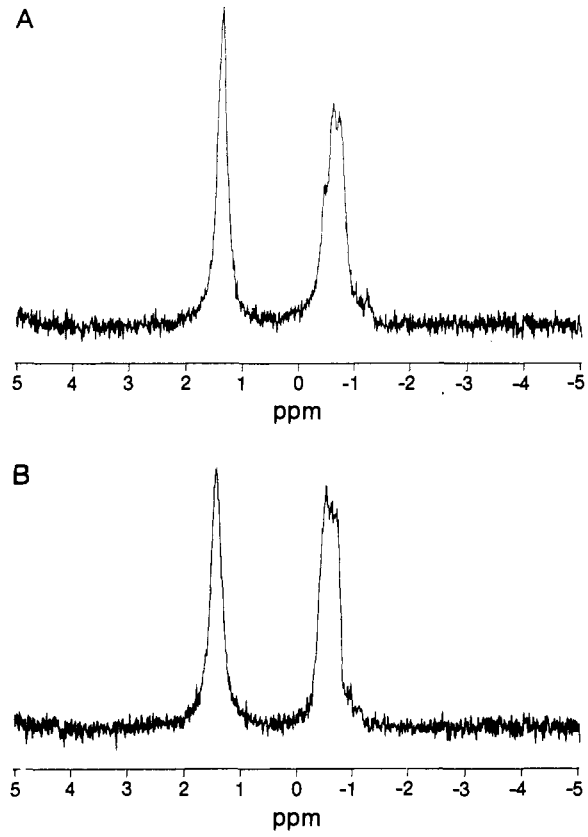

FIGURE 9: One-dimensional ^{31}P spectra of the α-DNA·β-RNA duplex at 5 (A) and 20 °C (B). Two distinct ^{31}P chemical shift ranges are apparent in the large peak on the right due to the ^{31}P resonances of α- and β-nucleosides at both temperatures. The large peak on the left is inorganic phosphate.

onances of the β-RNA strand. The assignment of the proton resonances of the β-RNA strand can be accomplished best by interpretation of the COSY spectra for much the same reason. The β-RNA strand has many strong scalar coupling interactions between protons grouped in such a way that informative regions of the spectra contain cross peaks only from the β-RNA strand. All six interactions are represented as strong cross peaks in the COSY spectrum. The H2′–H3′ interactions and H3′–H4′ interactions likewise are present for all six β-ribonucleosides in the COSY long-range experiment. Although the spin systems for all the β-ribonucleosides could all be isolated, the absence of interresidue NOEs made their sequential assignment impossible. It was possible to separate the purines from the pyrimidines on the basis of H6–H5 scalar and dipolar coupling interactions and to assign the 5′-terminal adenosine on the basis of the temperature dependence of its chemical shifts, since the molecule melts from the 5′-terminus. It was also possible to assign the 3′-terminal U on the basis of its upfield 3′-proton chemical shift. The two remaining uridines and the two guanosines are not distinguishable, however, and the chemical shift values listed in Table I for these pairs of nucleosides could be reversed.

^{31}P Studies. The one-dimensional ^{31}P spectrum of the β-RNA·α-DNA hybrid at 5 °C is shown in Figure 9. In contrast to ^{31}P spectra of β-DNA and β-RNA duplexes, there are two distinct regions to the spectrum. The more upfield region has fine structure and clearly several ^{31}P nuclei are resonating in this region. Both the upfield and downfield regions have roughly the same intensity, indicating the same number of ^{31}P resonances are contained in each region. One possibility consistent with the observed spectrum is that the α-DNA and β-RNA phosphates have intrinsically different shifts. A second possibility is that the phosphate shifts of each strand are sequence or residue dependent and that both α-DNA and β-RNA phosphate shifts are contained in each region. If the phosphate shifts are sequence or residue dependent, but not dependent upon incorporation in an α-DNA or β-strand, the two regions observed in the ^{31}P spectrum at 5 °C should coalesce into a single region as the temperature is raised and the duplex is melted into its constituent strands. In Figure 9B is also shown the ^{31}P spectrum of the α-DNA·β-RNA hybrid at 20 °C. Studies of the imino protons indicated fast exchange for all imino protons at 20 °C. The ^{31}P spectrum at this temperature clearly indicates that two regions are present. Thus the two regions of the ^{31}P spectrum are probably due to intrinsic differences in the ^{31}P chemical shifts of α-DNA and β-RNA nucleotides. It was observed that the fine structure present in the two regions at lower temperature remained in the spectra obtained at higher temperatures, indicating some sequence specificity in the ^{31}P chemical shifts. The intrinsic difference in ^{31}P chemical shifts between the α-DNA and β-RNA shifts could be the result of the α-DNA strand favoring a gauche-gauche conformation rather than a trans-gauche. Certainly the chemical shift differences result from changes in torsional angles about the phosphate backbone rather than ring current effects. This point is substantiated by the similarity in chemical shifts for H1′ of the α-DNA and β-RNA strands at a position more susceptible to ring current effects.

In order to correlate the ^{31}P resonances with ^{1}H resonances in each nucleotide, a heteronuclear multiple quantum correlation experiment was run at 5 °C. The delay used was optimized for a 10-Hz ^{31}P–^{1}H coupling constant. The spectrum is shown in Figure 8. Clearly evident in the spectrum is the same two-region separation of the α-DNA and β-RNA ^{31}P shifts. The corresponding H3′ resonances also are found in distinct regions in the α-DNA and β-RNA strands. The more upfield H3′ resonances were assigned to the α-DNA strand while the downfield resonances are due to H3′ of the β-RNA strand by ^{1}H–^{1}H correlation methods (vide supra). In neither the α-DNA nor the β-RNA strand were correlations to H5′ or H5″ observed. The ^{1}H–^{31}P couplings to H5′ must be sufficiently different from 10 Hz such that very little multiple-quantum coherence is developed between the ^{31}P resonances and H5′.

Analysis of Sugar Pucker with the α-DNA·β-RNA Hybrid. The conformation of the sugar may be deduced from NOEs from base protons to sugar protons and NOEs between sugar protons, while complementary information can be derived from observed scalar couplings among the sugar resonances. The conformation of the α-deoxynucleosides in the α-DNA·β-RNA hybrid must be analyzed solely by the observed NOEs because the couplings from H2′ and H2″ to both H1′ and to H3′ cannot be measured by the usual methods. No scalar coupling could be detected for these interactions in either the *J*-resolved or the magnitude, phase-sensitive, or long-range COSY experiments under conditions where the molecule existed as a stable duplex. One possibility for the absence of the cross peaks corresponding to these interactions would be rapid relaxation of the H2′ spins. A T_1 analysis did show the H2′ positions to relax quickly with a T_1 of 0.25 s. The thymidine methyl group relaxed as quickly and a coupling was still observed in the *J*-resolved experiment, although it was of low intensity, especially when considering it arose from three identical spins. Further evidence that relaxation effects are a cause of the undetectability of the expected interactions in the COSY and *J*-resolved spectra for the α-deoxynucleosides

Table II: Coupling Constants for β-RNA Nucleosides

	H1′–H2′	H2′–H3′	H3′–H4′	H3′–^{31}P
A7	7	≤3	≤3	6
U8	10	≤3	≤3	7
G9	9	≤3	≤3	11
U10	10	≤3	≤3	7
G11	9	≤3	≤3	11
U12	9	≤3	≤3	7

Table III: Average Relaxation Time (T_1) Values for the Components of the α-DNA·β-RNA Hybrid

	α-DNA	β-RNA
H1′	0.8	0.8
H2′	0.3	0.6
H3′	0.3	0.3
H4′	0.3	0.3
H8/H6	0.8	0.6

is the absence of cross peaks due to the H2′–H2″ interactions, which must have a large vicinal coupling. Cross peaks for the H2′–H2″ interactions were observed in COSY spectra taken with coarse digital resolution in F1 but only weakly in well-digitized spectra, where relaxation effects are pronounced. The appearance of intense H2′–H2″ cross peaks in well-digitized NOESY spectra, which has the same incrementing of the evolution time as does the COSY experiment, indicates a different sensitivity to T_2 effects in the two experiments. Both relaxation effects and small couplings from H2′ and H2″ to both H1′ and H3′ are factors in the undetectability of the corresponding cross peaks.

In contrast to the undetectability of the cross peaks from H2′ and H2″ to both H1′ and to H3′ for the α-deoxynucleosides in NMR experiments designed to detect scalar couplings, the analogous cross peaks for the β-ribonucleosides are readily apparent. In fact the sensitivity of the experiment was good enough to detect the lesser form of the duplex, which was present in only about 20% concentration. ^{1}H–^{1}H scalar couplings for the β-ribonucleosides were measured directly from the J-resolved spectrum or measured from the cross-peak fine structure of the ^{31}P-decoupled phase-sensitive COSY spectrum (Figure S4). The H1′–H2′ cross peak was a simple four-peak pattern expected of an AX spin system rather than the eight-peak pattern characteristic of the AM cross peaks of an AMX spin system (Hosur et al., 1988). This indicates that the H2′–H3′ coupling is small relative to the digital resolution of the spectra, which was 3.2 Hz/point. This was true for all the ribonucleosides of the β-RNA strand. The couplings between H1′–H2′ were measured directly from the center of one component of the cross peak to the center of the second antiphase cross-peak component and were not corrected for line shape. The H2′–H3′ coupling, which was not apparent in the multiplet, was estimated at less than 3 Hz. The H2′–H3′ coupling is nonzero, since the corresponding cross peak is visible in the long-range COSY experiment. The coupling between H3′ and H4′ also appeared to be less than the digital resolution of the spectrum and was estimated at less than 3 Hz. This coupling, too, is nonzero as evidenced by the corresponding cross peak in the long-range COSY experiment. One of the couplings to H3′ was well resolved in the ^{1}H–^{31}P correlation experiment and was about 3 Hz for all the β-ribonucleosides, while the second coupling is quite small. In all probability it is the H2′–H3′ coupling that is about 3 Hz and the H3′–H4′ coupling is small but the data could not distinguish between the two. The couplings are listed in Table II.

The geometry of the sugar was determined by using the pseudorotational analysis of deLeeuw and Altona (1982). The combination of relatively large scalar couplings between H1′ and H2′, moderate scalar coupling between H2′ and H3′, and small scalar couplings between H3′ and H4′ found for all the β-RNA nucleotides is characteristic of a pseudorotation angle near 144°, which correspond to a $^2T_1$ twist conformation. The amplitude of the sugar pucker appears to be large, greater than 40° and for some sugars near 50°. This sugar pucker is of the "S"-type characteristic of the "B" family of DNA helices indicating that, in contrast to RNA·DNA hybrids involving strictly β-nucleosides, hybrids involving α-nucleosides do not necessarily adopt an "A"-form geometry.

The sugar puckers of the α-DNA strand could not be determined from an analysis of coupling constants as could the sugar conformations of the β-RNA strand due to relaxation effects. The nature of the more rapid relaxation of the α-DNA H2′ and H2″ positions compared to the H2′ position of the β-ribose would be of interest to explore further. The T_1 values for comparable positions of the α-deoxyribonucleotides and the β-ribonucleotides are summarized in Table III. The most pertinent features of the sugar geometry of the α-DNA strand are accessible from the NOE data. The conformation about the glycosidic bond is anti as evidenced by strong NOEs from the base proton to H4′. The sugar pucker must be $^2T_1$ if it is a twist or ^2E if an envelope to account for the absence of NOEs from the base proton to either H2′ or H2″ for in these sugar pucker modes the base proton to C2′ proton distance is maximum. The sugar pucker of the α-deoxynucleosides, as well as the β-ribonucleosides, are of the S type in the α-DNA·β-RNA hybrid.

An analysis of the ^{31}P–^{1}H couplings from the ^{31}P-^{1}H correlation experiment revealed that while the ^{31}P chemical shifts for the two strands of the α-DNA·β-RNA hybrid are different, the three-bond couplings involving H3′ are much the same. The coupling constants for the β-RNA strand range from 7 to 10 Hz, while those from the α-DNA strand range from 6 to 11 Hz. This indicates that the chemical shift difference of phosphorus in the two strands does not arise from a difference in torisonal angles about the phosphate backbone, which affect the scalar coupling to H3′. There are two ranges of C3′–O3′ torsional angles consistent with the ^{31}P–^{1}H couplings and these can be determined from a Karplus-type relation $J = 16.3 \cos^2 \phi - 4.6 \cos \phi$ (Chary et al., 1989) to be centered around $\phi = 148$ and $\phi = 55$. The α-DNA and β-RNA strands may adopt conformations in these two ranges, resulting in distinct chemical shifts but similar ^{31}P–H3′ J-couplings. The ^{1}H–^{31}P couplings are included in Table II.

Molecular Modeling. The α-DNA·β-RNA duplex was modeled by using MIDAS and CHARMm by first creating both A- and B-form models of the corresponding antiparallel duplex of β-DNA strands from the coordinates of Arnott and Hukins (1972), generated from the program MAKE.DNA. The geometry of the sugars of both strands was then modified to reflect the conclusions drawn from the NMR structural analysis. A FORTRAN program was written to generate the atomic coordinates in Cartesian space from the pseudorotation parameters known from the NMR analysis. The values input were a pseudorotation phase of 144° and an amplitude of puckering of 40°. The program generated nearly identical atomic coordinates for sugars whether the geometry of the sugar used as input was from the A or B model. The modified atomic coordinates of the sugars in both strands of both models were calculated and then put into position of the original A and B sugars, whie conserving the coordinates at C1′ and the relative orientation of the C1′–C4′ axis and the C1′–O4′–C4′ plane. A FORTRAN program for doing this was written and the new

models were then displayed in MIDAS. Hydrogens were added to the carbon skeleton by using the routines in the CHARMm program. The deoxyribose sugar of the β-RNA strand was then converted into a ribose by substituting a hydroxyl for H2″, while conserving the bond angles but increasing the bondlength to 1.43 Å. The β-deoxyribose of the α-DNA strand was then converted into an α-deoxyribose by implementing a short FORTRAN program that rotated the entire sugar and the 5′-phosphate about the C1′–C4′ axis. The rotation done in this way resulted naturally in formation of a parallel duplex structure.

The model resulting from these modifications maintained the geometry of the base pairs inherent in the A and B models and the original coordinates of C1′ for all nucleosides. The model also displayed realistic geometry for the sugars of both the α-DNA and the β-RNA strands. The model, however, did not display realistic bond distances and bond angles for the phosphate backbone. The distortion about the phosphate backbone could be alleviated by rotation about the glycosidic bond angle, χ. The extent to which the distortion could be reduced was highly model and strand dependent. The α-DNA strand of the B model could be brought into a distortion-free state by a rotation of -33.5° about χ. The β-RNA strand of the "B" model could be very much improved, but not made completely free of distortion, by a rotation of -25° about χ. A FORTRAN program to generate atomic coordinates for the nucleosides with the optimized values of χ was written and the resulting model was displayed in MIDAS. The distortion about the phosphate backbone in the A model could not be alleviated nearly as well by rotation about χ.

The models created in this way all meet the constraints imposed by the NMR structural analysis. In particular, they are all representations of a parallel hybrid double helix and they all have sugar puckers consistent with the pseudorotation parameters determined from an analysis of the *J*-couplings in the phase-sensitive COSY experiment. The model also represents accurately the pattern of NOEs observed from base to sugar protons in the parallel hybrid duplex. In particular, the model predicts that interresidue NOEs from base protons to the sugar protons (H1′, H2′, H2″, and H4′) of the preceding and subsequent residues should be negligible because of the distances between these atoms. The NOESY experiments, even with long mixing times, did not detect any of these NOEs except near the 5′-terminus, which was partially melted at 5 °C. The model also predicts that intraresidue NOEs between base protons and H4′ and H1′ should be observable and the NOE data are in agreement with this aspect of the model as well.

Modeling of the antiparallel hybrid duplex was accomplished in much the same manner as the modeling of the parallel species. The fundamental difference in the approach to modeling the antiparallel duplex is in the way the α-DNA strand is generated. In modeling the parallel duplex, the entire sugar (except H1′) and 5′-phosphate were rotated about the C1′–C4′ axis and new H1′ coordinates were generated on the basis of tetrahedral bonding about C1′. To generate the antiparallel duplex, the connectivity of the sugar to base was altered so that the sugar of the *N*th base in the original model becomes connected to the $N + 1$ base of the antiparallel α-DNA·β-RNA hybrid duplex in the new model. The resultant distortion in base to C1′ bond lengths was remedied by writing a FORTRAN program that translated the entire α-DNA strand about the long axis of the duplex.

The restrained molecular mechanics routines of the CHARMm program were used to generate energy-minimized molecular structures. The B DNA model for both the parallel and antiparallel structures were subjected to conjugate gradient minimization until a converged structure was arrived at. The restrained molecular mechanics was run at a temperature of 300 K and with a scaling factor of 1 for the constraints. Energy minimizations were done with and without the presence of 1000 water molecules. The dihedral angles of the ribose sugar were constrained to values consistent with the pseudorotation phase angle of 144° determined from the coupling constant data. Target constraints for internuclear distances were input in accordance with the NOE studies. In particular, intraresidue base proton to H1′ and H4′ distances were constrained to distances consistent with the medium to strong NOE cross-peak intensities observed for these interactions, and interresidue base proton to H2″ distances were constrained to be too large for cross peaks from these interactions to be observed in the NOESY spectrum. Converged structures were obtained with 1200 steps of conjugate gradient energy minimization for the structures without water and 2000 steps when water was included. The energy minimized structure for the "B" helix of parallel orientation, which is the major species in solution, is shown in Figure 10.

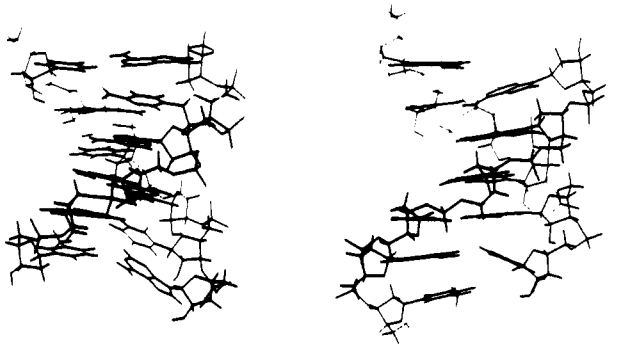

FIGURE 10: Depiction of the energy minimized structures for (left) the parallel α-DNA·β-RNA hybrid and (right) the antiparallel component of the α-DNA·β-RNA hybrid.

Evaluation of the energies for the two orientations shows the parallel structure is preferred over the antiparallel by a substantial amount. This is consistent with the energy-minimization studies of Sun et al. who found that for B-type hybrid helices the parallel orientation is the more stable. The NMR evidence is consistent with a B helix of parallel orientation. The NMR evidence also demonstrated a lesser component structure in equilibrium with the parallel B form. The low concentration of the lesser component made its complete structural assignment impossible, but the large energy gap between the favored parallel and disfavored antiparallel structures makes it unlikely that it forms a B-type helix. The energy minimization calculations of Sun et al. demonstrate that antiparallel orientations prefer A-type helices and our own calculations support this finding. Although there is not sufficient structural evidence to be certain, the lesser component in equilibrium with the B-form, parallel duplex is probably an antiparallel duplex of an A type as shown in Figure 10.

Annealing Experiments. It is evident from the ^{1}H NMR results that two species exist in equilibrium in solution for the hybrid α-5′-d[TACACA]·β-5′-r[AUGUGU] in an approximate of 4:1. The question of the polarity of annealing of α-DNA·β-RNA hybrids has been somewhat controversial. Recently a consensus view has developed that the polarity of annealing in such hybrids is, in general, parallel (Imbach et al., 1988). However, there are indications that the polarity of annealing is, to an extent, dependent on the particular sequences involved (Sun et al., 1988). The possibility of the

two alternative orientations of annealing arises with β-r[AUGUGU] and α-d[TACACA], owing to the purine–pyrimidine alternation. Therefore we examined the annealing of these and related pairs of sequences by thermal denaturation methods. As may be seen from Figure S5, β-r[AUGUGU] is able to hybridize with both α-d[TACACA] and the corresponding reverse sequence α-d[ACACAT]. In both cases, thermal denaturation curves of equimolar mixtures of β-RNA and α-DNA exhibit similar half-transition temperatures (T_m ~12 °C) under these conditions, although the β-r[AUGUGU]·α-d[TACACA] exhibits higher hyperchromicity. These results lend support to the ^{1}H NMR analysis, which indicates a 4:1 equilibrium between parallel and antiparallel annealed duplexes.

The thermal stability of three additional RNA·DNA hexamers was examined (Figure S5). These structures have in common the RNA strand of β-r[AUGUGA], which exhibits less pyrimidine–purine alternation than β-r[AUGUGU]. The antiparallel β-r[AUGUGA]·β-d[TCACAT] and parallel β-r[AUGUGA]·α-d[TACACT] duplexes exhibit similar stability (T_m ~8 °C), whereas the antiparallel β-r[AUGUGA]·α-d-[TCACAT] mixture shows a T_m (if any) lower than 0 °C. In the cases of all three of these duplexes, a reverse orientation of the two strands is unlikely because of only three points of recognition:

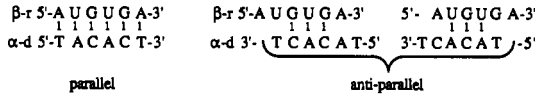

In contrast the present hybrid exhibits a maximum of five points of recognition in the antiparallel form

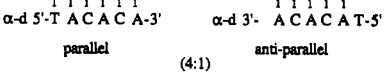

The results indicate that sequences of prospective targets need to be considered in the possible use of α-oligodeoxynucleotides as gene probes in order to ensure unambiguous parallel annealing, especially when at least five points of recognition exist in the opposing antiparallel hybrid. However, it should be emphasized that, up to now, antiparallel annealing between complementary α-DNA and β-RNA strands has only been found with homopyrimidine (Sun et al., 1988) or alternating purine–pyrimidine sequences (this work). This antiparallel orientation might have resulted from the formation of base pairs involving non Watson–Crick hydrogen-bonding interactions in the particular models. In fact, stable, parallel-stranded β,β-DNA resulting from reverse Watson–Crick base pair formation was predicted and experimentally observed in AT stretches (Pattabiraman, 1986; Van de Sande et al., 1988; Ramsing et al., 1988, 1989; Shchyolkina et al., 1989; Rippe et al., 1989). Furthermore, a single alteration of alternating purine–pyrimidine arrangement at the hexamer level is able to cancel the capability of an α-oligodeoxynucleotide to hybridize in antiparallel orientation to its complementary β-RNA strand, as exemplified above with β-r(AUGUGA)·α-d(TCACAT). Operationally of course both parallel and antiparallel annealing may be equally effective in masking a gene sequence but this has yet to be demonstrated.

Discussion

RNA duplexes and RNA·DNA hybrid duplexes generally adopt α-type helical geometries (Dock-Bregeon et al., 1989, Chou et al., 1989). A-type helices are characterized by C3′-endo sugar puckers, which increase base tilt and result in shorter interphosphate distance than in B helices. The preference for the C3′-endo sugar pucker for RNA helices stems from the intramolecular hydrogen bonds that form between the 2′-hydroxyl of the ribose sugar and the C2 oxygen of pyrimidine bases or the N3 nitrogen of purine bases for ribonucleotides with anti conformations about the glycosidic bond (Wang et al., 1982; Dock-Bregeon et al., 1989). The glycosidic bond conformations for the ribonucleosides of the α-DNA·β-RNA hybrid duplex are not strongly anti with values ranging from 300° for U8 to 248° for G11. In this range of values for χ, the O2′–O2 or O2′–N3 distances are too great for a bridging water molecule to stabilize the conformation. Instead the ribose sugar adopts a C2′-endo sugar pucker, which brings the 2′-hydroxyl to within 2.92 Å of the phosphate oxygen of the internucleotide linkage to the 3′-neighbor. This distance is within the range of a bridging water molecule to stabilize this conformation, and restrained molecular mechanics calculations including 200 bulk solvent molecules place bridging water molecules at these positions.

The energy minimized structure that resulted from restrained molecular mechanics on the parallel B-form duplex had a pattern of torsional angles that resemble Z DNA in that the values alternate depending on whether the 3′-residue is a purine or pyrimidine. The α-DNA·β-RNA duplex is right handed as evidenced by the NOE observed between H8 of A2 and the thymidine methyl group of T1, its 5′-neighbor. Sequences of α-DNA adopting a right-hand helical form are known to give interresidue NOEs from base protons to 5′-thymidine methyl groups (Lancelot et al., 1987) in contrast to β-DNA sequences in which the interresidue base proton to thymidine methyl group is to the 3′-neighbor (Feigon et al., 1983). The energy-minimized structure of Figure 10 also adopts a right-handed helical structure. The torsional angles about the phosphate backbone are dependent on the 3′-residue of the internucleotide link being either a purine or a pyrimidine in contrast to other right-handed helical structures such as A or B DNA (Saenger, 1984). In the β-RNA strand the O3′–P–O5′–C5′ (α) torsional angles for 3′-uridine dinucleoside units are ≈90° greater than for 3′-adenosine dinucleoside units. In the α-DNA strand the α torsional angles for 3′-adenosine dinucleoside units are 90° larger than for 3′-cytidine dinucleoside units. The systematic variance is not as large as in Z DNA, which varies by 180°, but it is significant and consistent. No systematic variance was input into the starting geometry, but one was always found independent of the constraints used in the molecular mechanics process. Systematic variance is found for the torsional angles α and β of both the α-DNA and β-RNA strands and also for the torsional angle ξ of the β-RNA strand. The torsional angles for the α-DNA and β-RNA strands are summarized in Table IV along with torsional angles for A, B, and Z DNA and A RNA.

NMR studies of RNA·DNA hybrids of both homopolymers and alternating pyrimidine–purine sequences have revealed B-type helical geometry for both strands of hybrid duplexes (Reid, 1983; Gupta, 1985). Recently, it was shown that α-(dT) binds β-(rA) preferentially in an antiparallel orientation, which calculations showed favors an A-type conformation (Sun et al., 1988). The stability of hybrid duplexes containing α-nucleosides is known to be sequence dependent, however (Imbach et al., 1988).

High-field ^{1}H and ^{31}P NMR analysis of the novel hybrid duplex α-d[TACACA] with β-r[AUGUGU] provided valuable structural information. The NMR revealed the existence of two forms in dynamic equilibrium in an approximate ratio of 4:1. The major component corresponds to parallel annealing

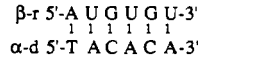

Table IV: Glycosidic Torsional Angles for the α-DNA·β-RNA Hybrid

3′-base	α	β	γ	δ	ϵ	ξ	χ
β-RNA							
U12	250	153	60	145	52	82	263
G11	165	181	59	144	217	190	248
U10	284	145	58	140	52	81	287
G9	168	192	58	146	220	163	242
U8	300	134	59	152			300
α-DNA							
A6	213	166	60	80	42	26	60
C5	141	92	27	75	52	50	73
A4	225	178	60	89	59	40	54
C3	174	216	58	88	59	46	62
A2	200	201	58	148			101
Z DNA[a]							
G	47	179	191	100	256	291	66
C	223	221	55	138	266	80	201
B DNA[a]	314	214	36	156	155	264	262
A DNA[a]	294	186	49	95	202	294	
A RNA[a]	285	208	45	83	178	313	

[a] From Saenger (1984).

while the minor component is ascribed to the antiparallel mode of binding in which there are five points of recognition:

β-r 5′-A U G U G U-3′
1 1 1 1 1
α-d 3′- A C A C A T-5′

This conclusion is in accord with thermal denaturation experiments. The major component clearly adopts predominately a B-type, parallel orientation as characterized by a C2′-endo sugar pucker and negligible interresidue base proton to H2″ NOEs (Chou et al., 1989). Northern blot experiments have indicated that only α-oligonucleotides designed to hybridize mRNA in a parallel orientation are able to hybridize to the target mRNA (Gagnor et al., 1989).

Considerable structural and stereochemical information on the major parallel component was deduced from the NMR analysis. The sugar pucker of the ribonucleosides was determined to be of the S type by pseudorotation analysis. The NOE pattern observed for the α-deoxyribonucleosides also suggested an S-type sugar pucker. The adoption of an S-type sugar conformation for both strands, which is also supported by the molecular modeling results, indicates that, in contrast to RNA·DNA duplexes formed exclusively from β-oligonucleotides, the α-DNA·β-RNA duplex appears to form a B-type helix.

The existence of a 20% contribution from the corresponding antiparallel hybrid, in which there are five points of base recognition, could be assigned to the alternating purine–pyrimidine arrangement of the selected sequence. Work is in progress to study the extent of possible antiparallel annealing in α-DNA·β-RNA duplexes. However, longer α-DNA sequences including the four natural bases in nonalternating arrangement have already been used for gene targeting, and parallel annealing with complementary RNA is well documented.

The B-type helix formed by the RNA strand of the α-DNA·β-RNA hybrid is not unprecedented for oligoribonucleotides but it may be sufficient to explain the RNase H resistance of the hybrid. Any number of parameters may influence recognition of the hybrid duplex by RNase H but one feature of a B-type duplex distinct from an A-type duplex is the greater interphosphate distance. It seems likely that an enzyme whose substrate adopts A-type helical geometry would contain electrostatic charges spaced to recognize the interphosphate distances of an A-type helix. The regular alteration in the torsional angles about the phosphate backbone may also influence the recognition of the hybrid duplex by RNase H. It would be of interest to know the helix type of the hybrid duplex formed between RNA and methyl phosphonate DNA. Neither the methyl phosphonates nor the α-oligonucleotides are ideal antisense agents because they are poor substrates for RNase H (Walder, 1988). Perhaps they also form B-type hybrid duplexes. In contrast, oligodeoxynucleotides with thiophosphate linkages are potent inhibitors of gene expression (Stein & Cohen, 1988), presumably because the hybrid duplex formed with mRNA is recognized by RNase H. A systematic study of the structures of hybrid duplexes of chimeric oligonucleotides that are potential antisense agents with RNA would be useful in revealing the structural features recognized by RNase H and in designing new antisense agents.

Acknowledgments

We thank Susan Gmeiner for assistance with the molecular modeling and energy minimization studies and Helmut Beirbeck and Alistair Muir for consultations in connection with the RING CLOSURE and MAKE.DNA programs, respectively.

Supplementary Material Available

Figures S1–S5 containing NOE difference spectra of the α-DNA·β-RNA hybrid, expansions of ROESY, NOESY, and COSY spectra, and a plot of optical density as a function of temperature for DNA·RNA hybrids (4 pages). Ordering information is given on any current masthead page.

Registry No. α-5′-d[TACACA]-3′·β-5′-r[AUGUGU]-3′, 129592-72-9; α-d[ACACAT]·β-r[AUGUGU], 129592-74-1; β-r-[AUGUGA]·α-d[TACACT], 129592-76-3.

References

Arnott, S., & Hukins, D. W. L. (1972) *Biochem. Biophys. Res. Commun. 47*, 1504–1509.
Aue, W. P., Bartholdi, E., & Ernst, R. R. (1976) *J. Chem. Phys. 64*, 2229–2246.
Bax, A. (1984) *J. Magn. Reson. 57*, 314–318.
Bax, A., & Freeman, R. (1981) *J. Magn. Reson. 44*, 542–561.
Bax, A., & Lerner, L. (1988) *J. Magn. Reson. 79*, 429–438.
Bax, A., Griffey, R. H., & Hawkins, B. L. (1983) *J. Magn. Reson. 55*, 301–315.
Bendall, M. R., & Pegg, D. T. (1983) *J. Magn. Res. 53*, 272–296.
Bertrand, J.-R., Rayner, B., Imbach, J.-L., Paoletti, C., & Malvy, C. (1989) *Biochem. Biophys. Res. Commun. 164*, 311–318.
Bodenhausen, G., Kogler, H., & Ernst, R. R. (1984) *J. Magn. Reson. 58*, 370–387.
Chary, K. V. R., Modi, S., Hosur, R. V., Govil, G., Chen, C.-Q., & Miles, H. T. (1989) *Biochemistry 28*, 5240–5249.
Chou, S.-H., Flynn, P., & Reid, B. (1989) *Biochemistry 28*, 2422–2435.
Cooney, M., Czemuszewicz, G., Postel, E. H., Flint, S. J., & Hogan, M. E. (1988) *Science 241*, 456–459.
deLeeuw, F. A. A. M., & Altona, C. (1982) *J. Chem. Soc., Perkin Trans. 2*, 375–384.
Dock-Bregeon, A. C., Chevrier, B., Podjarny, A., Johnson, J., deBear, J. S., Gough, G. R., Gilham, P. T., & Moras, D. (1989) *J. Mol. Biol. 209*, 459–474.
Feigon, J., Leupin, W., Denny, W. A., & Kearns, D. R. (1983) *Biochemistry 22*, 5943–5951.
Gagnor, C., Bertrand, J.-R., Thenet, S., Lemaitre, M., Morvan, F., Rayner, B., Malvy, C., Lebleu, B., Imbach, J.-L., & Paoletti, C. (1987) *Nucleic Acids Res. 15*, 10419–10435.

Gagnor, C., Rayner, B., Leonetti, J. P., Imbach, J.-L., & Lebleu, B. (1989) *Nucleic Acids. Res. 17*, 5107–5114.
Gautier, C., Morvan, F., Rayner, B., Huynh-Dinh, T., Igolen, J., Imbach, J.-L., Paoletti, C., & Paoletti, J. (1987) *Nucleic Acids Res. 15*, 6625–6641.
Gupta, G., Sarma, M. H., & Sarma, R. H. (1985) *J. Mol. Biol. 186*, 463–469.
Hare, D. R., Wemmer, D. E., Chou, S. H., Drobny, G., & Reid, B. R. (1983) *J. Mol. Biol. 171*, 319–336.
Harris, R. K. (1983) *Nuclear Magnetic Resonance Spectroscopy*, Pitman, London.
Hosur, R. V., Chary, K. V. R., Sheth, A., Girjesh, G., & Miles, H. T. (1988) *J. Biosci. 13*, 71–86.
Imbach, J.-L., Paoletti, C., & Lown, J. W. (1988) in *Structure and Expression Volume 2: DNA and Its Drug Complexes* (Sarma, R. H., & Sarma, M. H., Eds.) Adenine Press, Guilderland, NY.
Izant, J. G., & Weintraub, H. (1984) *Cell 36*, 1007–1019.
Kessler, H., Griesinger, C., Kergsebaum, R., Wagner, K., & Ernst, R. R. (1987) *J. Am. Chem. Soc. 109*, 607–609.
Lancelot, G., Guessner, J. L., Roi, V., & Thuong, N. T. (1987) *Nucleic Acids Res. 15*, 7531–7547.
Marion, D., & Wuthrich, K. (1983) *Biochem. Biophys. Res. Commun. 113*, 967–974.
Miller, P. S., & Ts'o, P. O. P. (1988) *Adv. Med. Chem. 23*, 295–312.
Miller, P. S., Yano, J., Yano, E., Caroll, C., Jayaramau, K., & Ts'o, P. O. P. (1979) *Biochemistry 18*, 5234–5245.
Mitchell, P. J., & Tjian, M. (1989) *Science 245*, 371–378.
Morvan, F., Rayner, B., Imbach, J.-L., Chang, D. K., & Lown, J. W. (1986) *Nucleic Acids Res. 14*, 5019–5035.
Morvan, F., Rayner, B., Imbach, J.-L., Thenet, S., Bertrand, J.-R., Paoletti, J., Malvy, C., & Paoletti, C. (1987a) *Nucleic Acids Res. 15*, 3421–3437.
Morvan, F., Rayner, B., Imbach, J.-L., Chang, D. K., & Lown, J. W. (1987b) *Nucleosides Nucleotides 6*, 471–472.
Morvan, F., Rayner, B., Imbach, J.-L., Chang, D. K., & Lown, J. W. (1987c) *Nucleic Acids. Res. 15*, 4241–4255.
Morvan, F., Rayner, B., Imbach, J.-L., Lee, M., Hartley, J. A., Chang, D. K., & Lown, J. W. (1987d) *Nucleic Acids Res. 15*, 7027–7043.
Morvan, F., Rayner, B., Leonetti, J.-P., & Imbach, J.-L. (1988) *Nucleic Acids Res. 16*, 833–847.
Paoletti, J., Bazile, D., Morvan, F., Imbach, J.-L., & Paoletti, C. (1989) *Nucleic Acids Res. 17*, 2693–2704.
Pattabiraman, N. (1986) *Biopolymers 25*, 1603–1606.
Post, M. L., Birnbaum, G. I., Huber, C. P., & Shugar, D. (1977) *Biochim. Biophys. Acta 479*, 133–142.
Ramsing, N. B., & Jovin, T. M. (1988) *Nucleic Acids Res. 16*, 6659–6675.
Ramsing, N. B., Rippe, K., & Jovin, T. M. (1989) *Biochemistry 28*, 9528–9535.
Redfield, A. G. (1976) in *NMR: Basic Principles and Progress 13*, Springer-Verlag, New York.
Reid, D. G., Salisbury, S. A., Brown, T., Williams, D. H., Vasseur, J.-J., Rayner, B., & Imbach, J.-L. (1983) *Eur. J. Biochem. 135*, 307–314.
Rippe, K., Ramsing, N. B., & Jovin, T. M. (1989) *Biochemistry 28*, 9536–9541.
Saenger, W. (1984) in *Principles of Nucleic Acid Structure*, Springer-Verlag, New York.
Sequin, U. (1973) *Experimentia 29*, 1059–1062.
Shaka, H. J., Keeler, J., & Freeman, R. (1983) *J. Magn. Reson. 53*, 313–340.
Shchyolkina, A. K., Lysov, Y. P., Il'ichova, I. A., Chernyi, A. A., Golova, Y. B., Chernov, B. K., Gottikl, B. P., & Florentiev, V. L. (1989) *FEBS Lett. 244*, 39–42.
Stein, C., & Cohen, J. (1988) *Cancer Res. 448*, 2659–2668.
Strickland, S., Huarte, J., Belin, D., Vassalli, A., Richler, R. J., & Vassalli, J.-D. (1988) *Science 241*, 680–684.
Sun, J., Francois, J.-C., Lavery, R., Saison-Behmoaras, T., Montenay-Garestier, T., Thuong, N. T., & Helene, C. (1988) *Biochemistry 27*, 6039–6045.
Ts'o, P. O. P., Rappaport, S. A., & Bollum, F. J. (1966) *Biochemistry 12*, 4153–4156.
Ts'o, P. O. P., Miller, P. S., & Greene, J. J. (1988) in *Development of Target-Oriented Anticancer Drugs* (Cheng, Y. C., Ed.) pp 189–206, Raven Press, New York.
Van de Sande, J. H., Ramsing, N. B., Germann, M. W., Elhorst, W., Kalisch, B. W., Kitzing, E. B., Pon, R. T., Clegg, R. C., & Jovin, T. M. (1988) *Science 241*, 551–557.
Vasseur, J.-J., Rayner, B., Pompon, A., & Imbach, J.-L. (1981) *Nouv. J. Chim. 5*, 343–347.
Walder, J. (1988) *Genes Dev. 2*, 502–504.
Wang, A. H. J., Fujii, S., van Boom, J. H., van der Marel, G. A., Van Boekel, S. A. A., & Rich, A. (1982) *Nature (London) 299*, 601–604.
Zamecnik, D. C., & Stephenson, M. L. (1978) *Proc. Natl. Acad. Sci. U.S.A. 75*, 280–284.
Zamecnik, P. C., Goodchild, J., Taguchi, Y., & Sarin, P. S. (1986) *Proc. Natl. Acad. Sci. U.S.A. 83*, 4143–4146.
Zon, G. (1988) *Pharm. Res. 5*, 539–553.